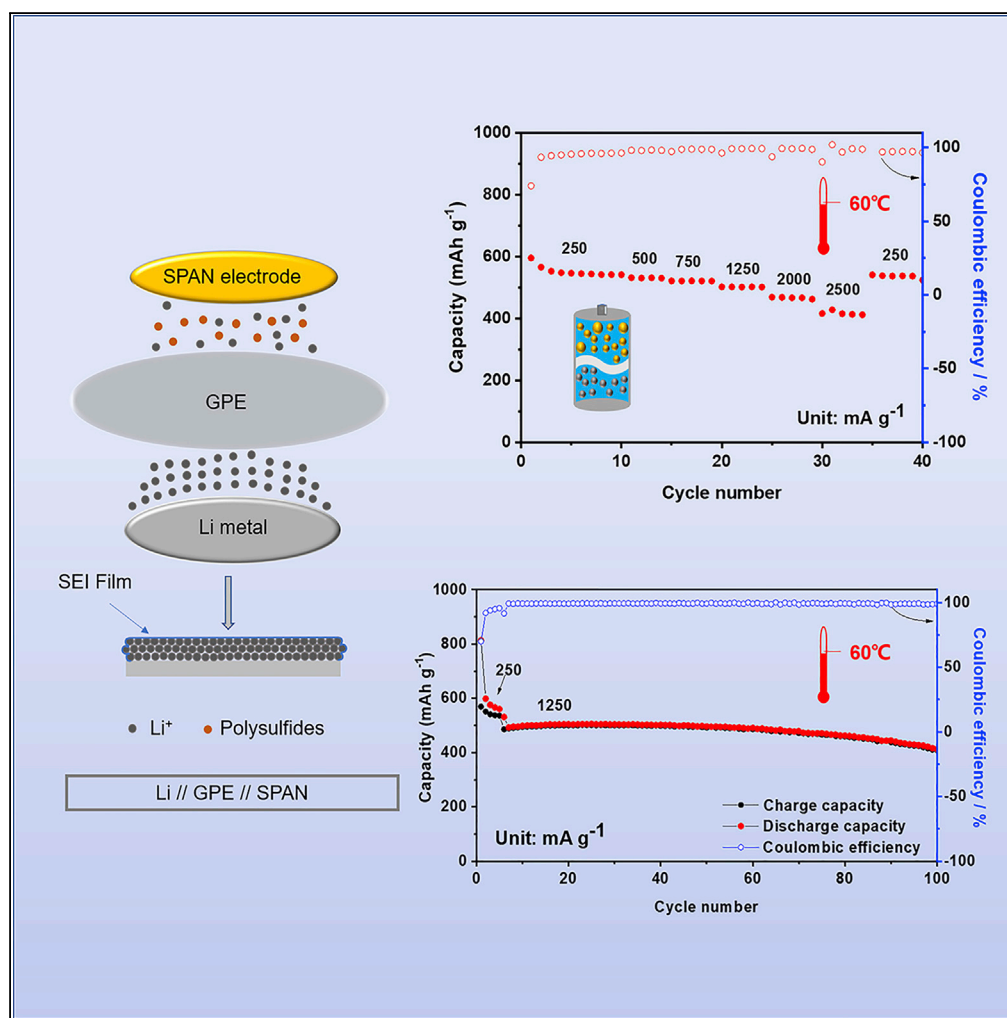## Article

Synergy of Sulfur/Polyacrylonitrile Composite and Gel Polymer Electrolyte Promises Heat-Resistant Lithium-Sulfur Batteries

Yu Liu, Dezhi Yang, Wenqi Yan, Qinghong Huang, Yusong Zhu, Lijun Fu, Yuping Wu

l.fu@njtech.edu.cn (L.F.)
wuyp@njtech.edu.cn (Y.W.)

HIGHLIGHTS

A Li-S battery with remarkable heat-resistant performance is obtained

Sulfur/polyacrylonitrile nanocomposites is used as positive electrode materials

Migration of polysulfides is observed during the cycling of the assembled battery

Gel polymer electrolyte is crucial for enhancing the performance at high temperature

Article

Synergy of Sulfur/Polyacrylonitrile Composite and Gel Polymer Electrolyte Promises Heat-Resistant Lithium-Sulfur Batteries

Yu Liu,[1,3] Dezhi Yang,[1,3] Wenqi Yan,[1] Qinghong Huang,[1] Yusong Zhu,[1] Lijun Fu,[1,2,4,*] and Yuping Wu[1,2,*]

SUMMARY

Lithium-sulfur (Li-S) batteries with high theoretical energy density attract great research attention. Although tremendous efforts have been made, heat tolerance capability of Li-S batteries is a topic rarely touched, although it is essential for practical application. At high temperatures, the dissolution of the polysulfides is aggravated, and the safety issue becomes severe. Herein, by using sulfur/polyacrylonitrile (SPAN) composites as positive electrode materials and a gel polymer membrane with carbonate electrolyte, we successfully realized a Li-S battery with remarkable heat-resistant performance at 50°C and 60°C. The SPAN-positive materials allow the Li-S battery operated in safer carbonate-containing electrolyte. The gel polymer electrolyte enhances the charge transfer, maintains the morphology of Li metal during cycling, and suppresses the migration of the soluble polysulfides, which is also observed when SPAN is used as positive electrode material. This contribution would bring new opportunity to extend the application of lithium batteries at high temperatures.

INTRODUCTION

Exploring better energy storage devices with high energy density, low cost, high safety, and long lifespan has boosted the development of new battery systems beyond the current mainstream lithium ion batteries (LIBs) (Bruce et al., 2012; Seh et al., 2016; Service, 2018). Among various alternative battery system candidates, Li-S batteries are considered one of the most promising electrochemical power sources. The cathode material (elemental sulfur), exhibits high theoretical specific capacity of 1,672 mAh g^{-1}, calculated from the reversible reaction $S_8 + 16\,e^- \rightarrow 8\,S^{2-}$, which enables Li-S batteries to achieve a high theoretical energy density of up to 2,600 W h kg^{-1}, five times higher than those of present LIBs (Dong et al., 2018; Li et al., 2018a, 2018b, 2018c, 2018d; Sun et al., 2016; Zhou et al., 2015). In addition, sulfur, as one of the key materials of various industries, is naturally abundant, has low cost, and is environment friendly when compared with the commercial cathode materials such as $LiCoO_2$, and $LiFePO_4$ (Umeshbabu et al., 2019; Yang et al., 2018a, 2018b). However, the practical application of Li-S batteries is still plagued with numerous challenges, such as the insulating nature of elemental sulfur and the discharge product (Li_2S). Besides, lithium polysulfides (LiPSs), which are generated by a multi-electron conversion reaction and easily dissolvable into the electrolyte, would cause shuttling effect between the two electrodes and form a passivating layer on the surface of lithium metal anode, including insulating sulfide species (Li_2S, Li_2S_2). These phenomena result in fast capacity fading and low coulombic efficiency of Li-S batteries (Elazari et al., 2011; Song et al., 2015).

Various attempts, such as cathode modification (nanostructure (Li et al., 2017a, 2017b; Yang et al., 2018a, 2018b), carbon-based composite (Gao et al., 2019; Hwa et al., 2017; Jayaprakash et al., 2011; Li et al., 2017a, 2017b, 2018a, 2018b; 2018c, 2018d; Yang et al., 2016, 2017), doping (Zhou et al., 2017), anode protection (Cha et al., 2018), electrolyte additives (Wang et al., 2018a), targeted binders (Li et al., 2015), and functional separators (Ghazi et al., 2017), have been proposed to regulate the behaviors of LiPSs. Metal oxides (Han et al., 2013; Zhou et al., 2013), sulfides (Chen et al., 2017; Cheng et al., 2018) or phosphide (M–O/S/P) (Zhong et al., 2018), and perovskite nanoparticles (Kong et al., 2018) have also been implemented to immobilize LiPSs and guide the Li_2S formation in Li-S batteries.

Besides the aforementioned challenges, heat tolerance of Li-S batteries is important for practical applications, yet not easy to realize, because the dissolution of the LiPSs is aggravated at high temperature, and the shuttle effect is strengthened as well (Busche et al., 2014). In addition, the safety concern of Li-S batteries at elevated temperature is essential, because of the low boiling and flash points of the commonly used

[1]State Key Laboratory of Materials-Oriented Chemical Engineering, College of Energy Science and Engineering and Institute of Advanced Materials, Nanjing Tech University, No.30, Puzhu Road (S), Nanjing, Jiangsu 211800, China

[2]School of Physics and Telecommunication Engineering, South China Normal University, No. 55, West Zhongshan Road, Tianhe District, Guangzhou, Guangdong 510631, China

[3]These authors contributed equally

[4]Lead Contact

*Correspondence: l.fu@njtech.edu.cn (L.F.), wuyp@njtech.edu.cn (Y.W.)

https://doi.org/10.1016/j.isci.2019.07.027

ether-based electrolytes (Li et al., 2016, 2018a, 2018b, 2018c, 2018d). So far only a few articles have touched upon this topic. Jin et al. designed a hollow Co_3S_4 nanobox with interconnected carbon nanotubes as the sulfur host and realized a cycle retention of 75.3% over 300 cycles at 335 mA g^{-1} at 50°C in an ether-based electrolyte (Chen et al., 2017). Zhang et al. entrapped sulfur into porous graphene and enabled the Li-S batteries operated at 60°C with a capacity of 551 mAh g^{-1}_{sulfur} at a current density of 1,672 mA g^{-1} (Huang et al., 2013). Regarding the safety concerns of the ether-based electrolyte, revisiting the traditional carbonate electrolyte would be an effective strategy. Sun et al. used molecular layer deposition method to coat aglucone on C-S electrode and enabled the Li-S batteries cycled in a carbonate electrolyte at a temperature range of −20°C to 55°C with high reversibility (Li et al., 2016, 2018a, 2018b, 2018c, 2018d).

A promising cathode material for Li-S batteries, sulfur/polyacrylonitrile nanocomposites (SPAN), was proposed (Wang et al., 2002, 2003) and allows a Li-S battery operated in a carbonate electrolyte (Wang et al., 2002; Wei et al., 2015). It can be synthesized by a facile annealing procedure with sulfur and polyacrylonitrile (PAN) as the mere raw materials, and the synthesis method can be easily scaled up. Although great efforts have been made, the structure of SPAN and its reaction mechanism during cycling are still controversial (Fanous et al., 2011; Frey et al., 2017; Hwang et al., 2013; Li et al., 2018a, 2018b, 2018c, 2018d; Liu et al., 2018; Wang et al., 2002, 2003, 2018a, 2018b; Wei et al., 2015).

Herein, we report a Li-S battery with excellent high-temperature performance, by using SPAN as positive electrode, and gel polymer membrane (GPM) soaked in carbonate electrolyte. The Li-S battery could be operated at a high temperature at 60°C; a high specific capacity of 547.8 mAh g^{-1} can be obtained at 250 mA g^{-1}, and even when the current density increases to 2,500 mA g^{-1}, a high reversible capacity of 415 mAh g^{-1} can still be retained. In addition, the electrochemical process of SPAN toward Li during cycling is discussed. The synergistic effects of SPAN and the gel polymer electrolyte (GPE) enable the excellent high-temperature behavior of Li-S battery, in terms of high energy density, rate capability, safety, and cycle stability.

RESULTS

Characterization of the Gel Polymer Membrane and SPAN

A polymer membrane containing polyvinylidene fluoride (PVDF) and polymethyl methacrylate (PMMA) was prepared and used in this study (please see Transparent Methods in Supplemental Information). The esters in the constitutional units of PMMA have good affinity with organic solvent molecules, which allows absorption of large amount of liquid electrolytes, which can provide the ionic conductivity. PVDF layer is introduced to guarantee the mechanical stability of GPE (Agnihotry et al., 2000; Vondrák et al., 2001). The GPM as prepared shows a considerable ionic conductivity of 0.74 × 10^{-3} S cm^{-1} (Figure S1) at room temperature after infiltration of liquid carbonate electrolyte, which is high enough for practical application. The ionic conductivity of the GPM increases as the temperature increases, because of the stronger motion of polymer local segments induced at high temperature. The GPE shows high ionic conductivity of 0.88 × 10^{-3} and 0.90 × 10^{-3} S cm^{-1} at 50°C and 60°C, respectively (Figure S1). Before being assembled into coin cell, the dry membranes (Celgard 2400 and polymer membrane) were punched into disks with a diameter of 19 mm as shown in Figures 1A and 1D. Representative scanning electron microscopic (SEM) images of top and cross-sectional view of both the membranes can be found in Figures 1B–1F. For the polymer membrane, the cross-sectional image (Figure 1F) indicates that the thickness of the membrane is ~20 μm. The electrolyte uptake of polymer membrane and Celgard 2400 is 113.2 wt. % and 86.5 wt. %, respectively. SPAN was prepared according to previous report (Liu et al., 2018; Wang et al., 2002; Wei et al., 2015). The structure of SPAN can be found in our previous study (Liu et al., 2018). The particle size of the as prepared SPAN is ~200 nm, and the morphology of the SPAN can be found in Figure S2. The specific surface area of SPAN is ~22.3 m^2 g^{-1}. The sulfur content in the composite is ~38 wt. %.

The electrochemical properties of Li-S batteries were characterized using CR2025 coin cells in the voltage range of 1.0–3.0 V (versus Li/Li⁺) at different temperatures, with SPAN as positive electrode material, lithium foil as negative electrode, and GPE and liquid electrolyte. The cells with gel polymer electrolyte and liquid electrolyte are denoted as CGPE and CLE, respectively.

Performance of the as Assembled Li-S Batteries at Room Temperature

The electrochemical performance of CLE and CGPE were investigated at room temperature first. At room temperature (RT), both CGPE and CLE exhibit similar charge/discharge profiles at 500 mA g^{-1} (Figures S3A
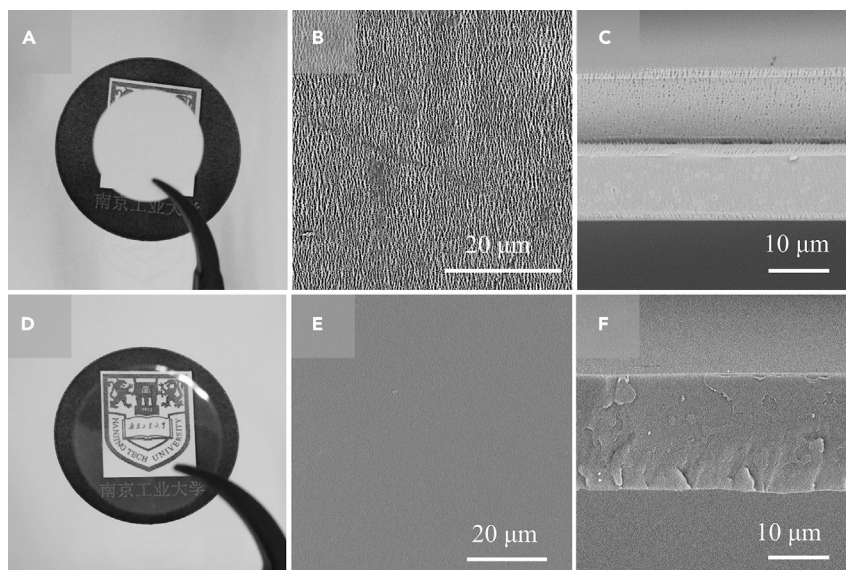
Figure 1. Morphology of Celgard 2400 and the Polymer Membrane
(A–C) Images of Celgard 2400 membrane. (A) Optical photograph, (B) top view, and (C) cross-sectional SEM images.
(D–F) Images of the gel polymer membrane. (D) Optical photographs, (E) top view, and (F) cross-sectional SEM images.
For Figures 1B and 1E, the scale bar is 20 μm, and for Figures 1C and 1F, the scale bar is 10 μm.

and S3B). A smooth discharge slope can be observed from 1.5–1.0 V during the first discharge process, which is different from the discharge profiles in the following cycles. This behavior is similar as the previous reports and it may be attributed to an activation process and structure rearrangement of SPAN during the first discharge (Hwang et al., 2013). The CLE shows good performance at room temperature (Fanous et al., 2011; Wei et al., 2015). The cycling performances of both CLE and CGPE at 500 mA g^{-1} are almost identical during the first 250 cycles, delivering a reversible capacity of ~428.1 mAh g^{-1}. CGPE presents better cycling stability than CLE. The reversible capacity is 426.6 mAh g^{-1} for CGPE over 500 cycles, 92.2% of its original capacity; whereas for CLE, only 376.7 mAh g^{-1} can be obtained after 500 cycles and capacity retention is 88%. SPAN electrode with the GPE exhibits excellent cycle performance at room temperature, as listed in Table S1. The rate performance of CGPE is superior to that of CLE as well; it delivers a reversible capacity of 492, 470, 456, 433, 404, and 390 mAh g^{-1} at current densities of 250, 500, 750, 1250, 2,000, and 2,500 mA g^{-1}, respectively. On the contrary, for CLE, the reversible capacities at corresponding current densities are 473, 451, 429, 402, 374, and 356 mAh g^{-1}, respectively. The superior performance of CGPE may be attributed to the good contact between GPE and both electrodes, which leads to faster kinetic property and good stability of both electrodes (Figure S4).

Excellent High-Temperature Resistance Capability

When the temperature is raised to 50°C, the electrochemical behaviors of CGPE and CLE present significant differences. The cycle performances of both cells at 250 mA g^{-1} are displayed in Figure 2A. The reversible capacities of CGPE are 553.6, 535.6, and 528.7 mAh g^{-1} for the initial three cycles. In the following cycles, the capacity of CGPE maintains at 526 mAh g^{-1}, with a coulombic efficiency above 99%. A reversible capacity of 501 mAh g^{-1} can be retained over 180 cycles, corresponding to high capacity retention of 90.6% and low capacity decay rate of 0.052% per cycle, and a reversible capacity of 470 mAh g^{-1} can be maintained after 200 cycles. For CLE, the reversible capacities of the initial three cycles are 513.3, 496.4, and 484.2 mAh g^{-1}, respectively. It exhibits poor cycling performance; only 319.5 mAh g^{-1} and 246.1mAh g^{-1} are retained over 100 and 200 cycles, i.e., 62.3% and 47.9% of its original capacity, respectively. The results from the galvanostatic investigation of both cells at 250 mA g^{-1} and 50°C are consistent with the cycling performance (Figures 2B and S5).

CGPE delivers excellent rate performance, when compared with CLE. As shown in Figure 2C, reversible capacities of 520, 500, 489, 469, 438, and 420 mAh g^{-1} can be obtained at 250, 500, 750, 1,250, 2,000, and 2,500 mA g^{-1}, respectively. When the current density is back to 250 mA g^{-1}, an additional rate performance
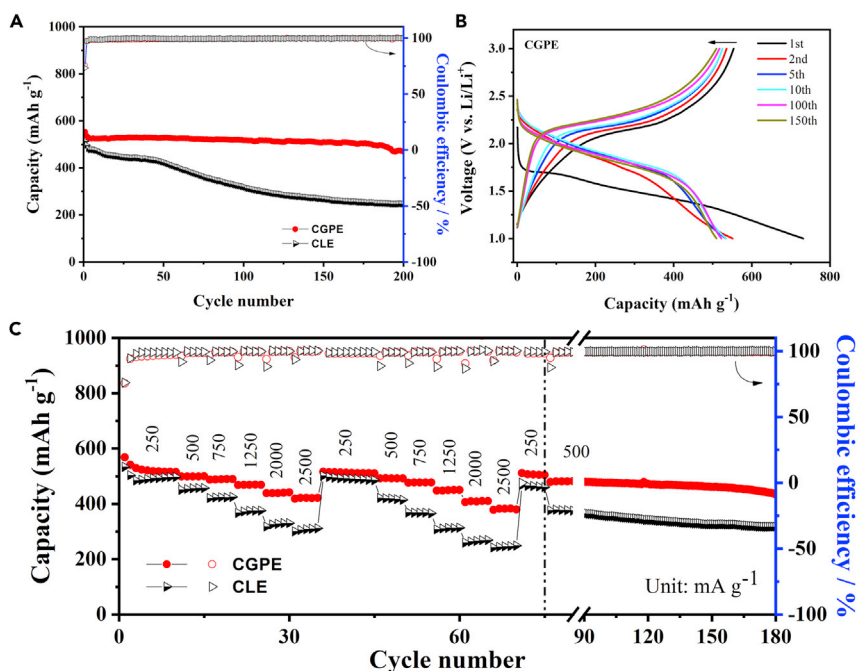
Figure 2. Electrochemical Characterization and Performance of CLE and CGPE at 50°C
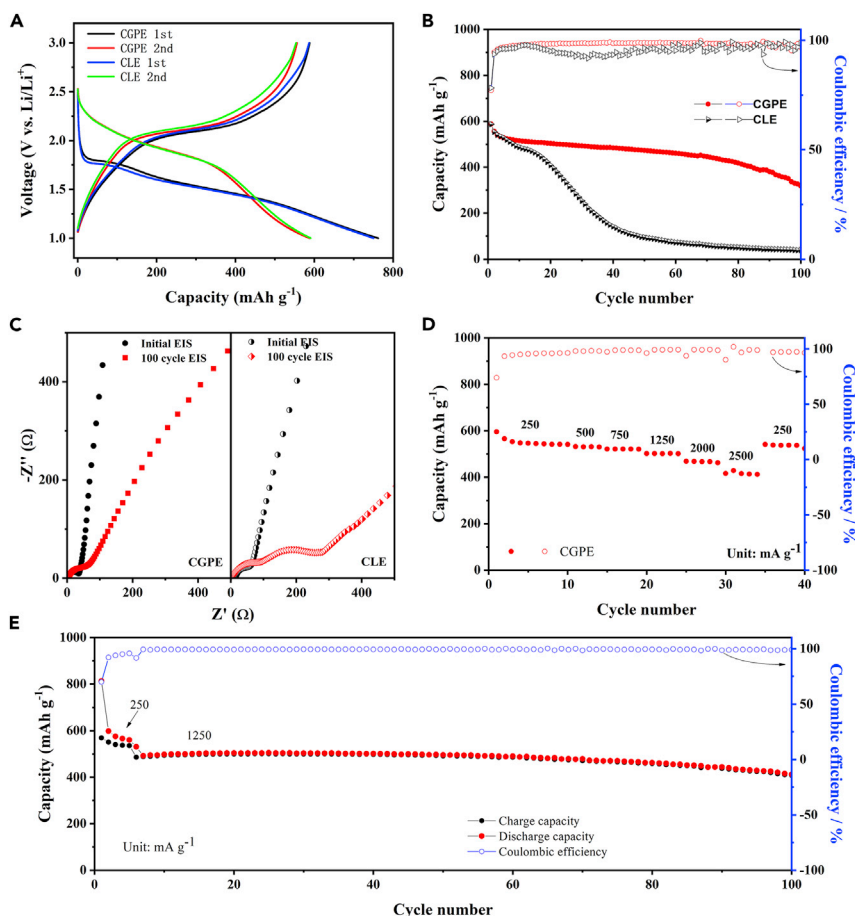(A) Cycling performance at 250 mA g^{-1}.
(B) Galvanostatic charge/discharge profiles of CGPE at different cycles.
(C) Rate performance of CLE and CGPE.

test was carried out by applying the current density in an ascending order; excellent rate performance of CGPE can still be obtained with reversible capacities of 510, 492, 477, 450, 410, and 382 mAh g^{-1} at 250, 500, 750, 1,250, 2,000, and 2,500 mA g^{-1}, respectively. When the current density is returned to 250 mA g^{-1}, a discharge capacity of 510 mAh g^{-1} can still be retained, demonstrating the good stability of the CGPE at 50°C under various current densities. Moreover, it maintains good cyclability during the subsequent 100 cycles at 500 mA g^{-1}, as shown in Figure 2C. In contrast, the cell with liquid electrolyte delivers lower capacities at various rates. The reversible capacities of the cell with liquid electrolyte are 497, 457, 424, 375, 327, and 308 mAh g^{-1} at 250, 500, 750, 1,250, 2,000, and 2,500 mA g^{-1}, respectively.

An extraordinary electrochemical behavior of CGPE can be achieved even when the temperature increases to 60°C (Figure 3). Both CGPE and CLE exhibit almost similar electrochemical performances during the initial two cycles at 250 mA g^{-1}. The initial discharge/charge capacities of CGPE and CLE are 762.6/588.2 and 750.2/587.1 mAh g^{-1} at 250 mA g^{-1} (Figure 3A), respectively, corresponding to a capacity of 1,955.3 mAh g$_{sulfur}$$^{-1}$ and 1,923.5 mAh g$_{sulfur}$$^{-1}$, calculated based on the sulfur content in SPAN. These discharge capacities exceed the theoretical capacity of sulfur, which can be attributed to the formation of the solid-electrolyte interlayer (SEI) film during the first cycle and side reactions between lithium and the surface functional groups, such as π-conjugated backbone of the SPAN, a well-known phenomenon that occurs in conductive polymers (Burkhardt et al., 2011; MacDiarmid, 2001; Otero and Cantero, 1999). Both cells show a slope profile from 1.8 to 1.0 V during the first discharge process, similar as those at RT and 50°C, suggesting that an activation process still occurs at 60°C.

Similar capacities can be obtained during the first few cycles for both CGPE and CLE (Figure 3B). In the subsequent cycles, CGPE presents excellent cycling performance and the reversible capacity remains at 473.4 and 418 mAh g^{-1} after 50 and 80 cycles at 250 mA g^{-1}, respectively, corresponding to high capacity retention of 80.5% and 71.1% and a low capacity decay rate of 0.39% and 0.36% per cycle. After 100 cycles, a reversible capacity of 318.4 mAh g^{-1} can still be maintained. Different from the behavior at 50°C, CLE suffers from severe capacity fading at 60°C. The reversible capacity is only 39.5 mAh g^{-1} over 100 cycles, corresponding to extremely low capacity retention of 6.7% and rapid capacity decay rate of 0.933% per cycle at high temperature. Detailed investigation of the galvanostatic profiles may lead to an insight into the

Figure 3. Electrochemical Characterization and Performance of CLE and CGPE at 60°C

(A) The initial and second charge/discharge galvanostatic profiles of CLE and CGPE.

(B) Cycling performance of CLE and CGPE at 250 mA g^{-1}.

(C) Nyquist plots of CLE and CGPE at the initial and the 100th cycles under 60°C.

(D) Rate performance of CGPE.

(E) Cycling performance of CGPE at 1,250 mA g^{-1} after cycling at 250 mA g^{-1} for five times.

phenomena. For CLE, after cycling for several times at 60°C, a saw-like charge curve (Figure S6) is observed, which may be ascribed to short-circuit of the cell at high temperature, whereas the same is not observed for CGPE. In addition, the resistances of both the cells increase after cycling for 100 cycles (Figure 3C), and the resistance increase for CLE is much larger than that of CGPE; this would also contribute to the poor cycling performance of the cell with liquid electrolyte. The good contact between gel polymer and both electrodes leads to smaller resistance of CGPE than that of CLE.

CGPE also exhibits an excellent rate capability at 60°C (Figures 3D and S7). The reversible capacities of SPAN in CGPE are 547.8, 531.7, 521.4, 502, 468, and 415 mAh g^{-1} at 250, 500, 750, 1,250, 2,000, and 2,500 mA g^{-1}, respectively. When the current density decreases to 250 mA g^{-1} again, a reversible capacity of 538 mAh g^{-1} still remains. The galvanostatic charge/discharge profiles of CGEP at different rates also demonstrate the remarkable rate performance (Figure S7). Excellent cycling stability of CGPE can also be achieved at 500 and 1,250 mA g^{-1} (Figures S8 and 3E), and the cycling performance at high temperatures is remarkable among those reported in literatures (Table S2). The reversible capacities of SPAN in CGPE are 567.6, and 539.4 mAh g^{-1} for the first two cycles at 500 mA g^{-1}, and a reversible capacity of 447.0 mAh g^{-1} with a Coulombic efficiency above 99% can still be retained after 100 cycles. The capacity retention is as high as 78.8%, and the corresponding capacity decay is 0.21% per cycle (Figure S8). When CGPE is cycled at 250 mA g^{-1} for five times, and subsequently cycled at 1,250 mA g^{-1}, a reversible capacity of 408 mAh g^{-1} can be maintained over 100 cycles, i.e., 84% of the initial reversible capacity.
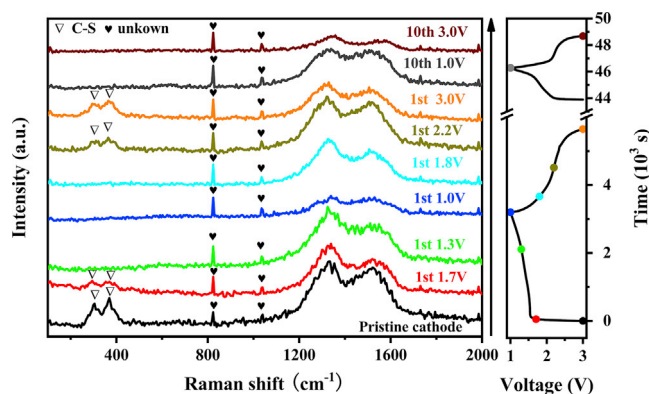
Figure 4. *Ex situ* Raman Spectra Study of SPAN at Different States during the First and 10th Cycles in CLE

Synergistic Effects of SPAN and the Gel Polymer Electrolyte

The structures of SPAN and that after cycling were proposed by different groups, yet they are still under controversy. For SPAN, it was proposed that sulfur was chemically bonded to carbon in SPAN, existing in the forms of oligo(sulfide)s (Liu et al., 2018; Wei et al., 2015), 2-pyridylthiolates (Wang et al., 2018b), and thioamide structures (Fanous et al., 2011). In addition, another molecular structure, in which a S_8 ring was coupled with four pyridine rings in SPAN, was also proposed (Doan et al., 2013). Apart from the structure, different reaction mechanisms of SPAN toward lithium were reported in the literature. Archer et al. claimed that the covalent S-C bond was broken after discharge process and recovered upon charge, and sulfur was maintained as smaller molecular S_3 and S_2 in SPAN during the cycling, which were trapped in the carbon matrix via covalent bonding or physical confinement (Wei et al., 2015). The cleavage and re-binding of the covalent bond were reported by Fanous et al. as well; however, they suggested that S_8 was present upon charge (Fanous et al., 2011). Wang et al. found that it was not the C-S bond, but the S-S bond of SPAN that was cleaved and thiyl radicals were generated to form a conjugative structure, which reacted with lithium reversibly consequently (Wang et al., 2018b).

To get a deep insight of the excellent electrochemical performance of CGPE at high temperatures, and understand the structure evolution of SPAN during cycling, the reaction process between SPAN and lithium was investigated via *ex situ* Raman, X-ray photoelectron spectroscopy (XPS), and energy-dispersive spectroscopy (EDS) mapping. Figure 4 shows that the *ex situ* Raman spectra of the SPAN electrode at different states during the first and 10th cycles at room temperature. For the pristine SPAN, the characteristic peaks are located at 1,340 and 1,558 cm^{-1}, ascribed to the D- and G-bands of carbon, respectively. Besides, two peaks can be observed at 297 and 372 cm^{-1}, which are attributed to the C-S bonds, indicating that sulfur is chemically bonded with the carbon matrix during the heat treatment (Fanous et al., 2011; Frey et al., 2017; Liu et al., 2018; Wei et al., 2015; Yu et al., 2004). The intensities of the C-S bond peaks vary significantly during cycling. During the first cycle, the intensities of C-S bond peaks decrease when discharge to 1.7 V, and the bond peaks disappear when the voltage reaches 1.3 V and further down to 1 V, whereas the bond peaks are present again when charged back to 2.2 V and their intensities increase along with the charge process till 3 V. Yet the intensity does not recover to its original status, indicating that the C-S bonds are cleaved after first discharge and reformed upon first charge and that the cleavage/reformation process is not fully reversible in the first cycle. This variation trend of the C-S bond peak intensities is similar with that reported by Archer et al. (Wei et al., 2015) and what we observed in a K-S battery using SPAN as cathode (Liu et al., 2018). In addition, the Raman spectra of the SPAN sample during the 10th cycle indicate that the C-S bond peaks vanish, at both discharge and charge states, suggesting that the C-S bond is cleaved completely and could not be reformed after 10 cycles maximally. The galvanostatic profiles provide other evidences. It is reported that the lower discharge plateau of the initial cycle is ascribed to the cleavage of C-S bond and rearrangement of the structure (Hwang et al., 2013). A careful observation of the discharge profiles at RT (Figure S3) shows that the average voltage of the discharge process increases during the first 10 cycles (Figure S3A), indicating that the cleavage of the C-S bonds continues; however, less activation energy is needed with cycling. It suggests that the C-S cleavage and reformation is not fully reversible. The average discharge voltage decreases again during the 100th cycle, which may be attributed to the polarization of the cell during cycling. Similar trend of the discharge curves can be found for CLE at 50°C (Figure S5). These

Content (wt. %)	CLE			CGPE		
	RT	50°C	60°C	RT	50°C	60°C
S	0.22	0.15	1.87	0	0	0.03
C	26.75	41.93	39.24	36.90	46.68	42.86
O	23.23	19.24	26.98	20.01	26.56	27.73
F	37.25	23.34	15.72	29.12	15.96	17.39
P	3.11	2.35	3.91	3.01	3.34	4.06
Li	9.43	13	12.28	10.96	7.47	7.39

Table 1. The Element Content on the Li Metal Surface in Li-S Batteries at Different Temperatures from RT to 60°C after 100 Cycles from XPS Analyses

results suggest that C-S bonds cleave and sulfur molecules are formed in the carbon matrix of SPAN during cycling. Specific design of the sulfur materials allows the operations of Li-S batteries in carbonate electrolyte (Gao et al., 2011; Xin et al., 2012). The confinement of sulfur in the carbon matrix would suppress the reaction between sulfur and carbonate. With the GPE, the restraint of the electrolyte may limit the reaction further, giving rise to good cycle performance of SPAN with carbonate-based electrolyte, especially for CGPE at high temperatures.

Surface analyses were performed on Li metal and the positive electrode in CGPE and CLE after cycling at different temperatures. Both XPS and EDS elemental analyses suggest that sulfur traces can be detected on the surface of Li metal at various temperatures (Tables 1 and 2). The amount of sulfur on Li metal increases when the temperatures for both CGPE and CLE increase. Especially, a significant boost of the sulfur amount can be observed when lifting the temperature from 50°C to 60°C. In addition, the sulfur amount on the surface of Li metal in CGPE is less than that in CLE at different temperatures in general. At 60°C in particular, the atomic ratios of sulfur on Li metal are 0.03% and 0.19% in CGPE, investigated via XPS and EDS, respectively, which are much less than those in CLE (Tables 1 and 2). The value discrepancy may be attributed to the different analysis techniques. The sulfur at the positive electrode was analyzed via XPS technique. At positions where no N element is observed, the sulfur element can still be detected, indicating that the sulfur detected is outside or in the SEI film, rather than in the SPAN material (Table S3). The amount of sulfur on the positive electrode does not follow the similar trend of Li metal, which might be ascribed to the dissolution of polysulfide in the electrolyte and the washing process of cycled SPAN with dimethyl carbonate (DMC) solvent.

The aforementioned results also suggest that dissolution of the polysulfide occurs when using SPAN as the positive electrode materials, which is promoted with the increase of temperature, and the dissolution can be mitigated effectively by the GPE (Figure 5). The dissolution phenomenon we observed might be ascribed to the reduction of sulfur molecules formed during cycling or its side reaction with carbonate electrolyte (Gao et al., 2011). There is little possibility that the dissolved polysulfide is from the residual sulfur during the preparation process, because the as prepared SPAN was evacuated at 200°C overnight. In addition, in a thermogravimetric analysis of SPAN under N_2, there is almost no weight loss in the temperature range of 100°C–400°C, indicating that there is little residual sulfur in SPAN (Figure S9) (Wang et al., 2018b).

Besides the suppression of polysulfide dissolution, the favorable kinetics of CGPE would also account for the excellent performance at high temperatures. The initial discharge profiles show that for both CGPE and CLE, the onset voltage is higher when raising the operation temperature (Figure S10), which is attributed to the decreased internal and charge transfer resistances at high temperature. A careful investigation reveals

Content (wt. %)	CLE			CGPE		
	RT	50°C	60°C	RT	50°C	60°C
S	0.29	0.55	2.25	0.04	0.1	0.19

Table 2. The Sulfur Content on the Li Metal Surface in Li-S Batteries at Different Temperatures from RT to 60°C after 100 Cycles from EDS Analyses
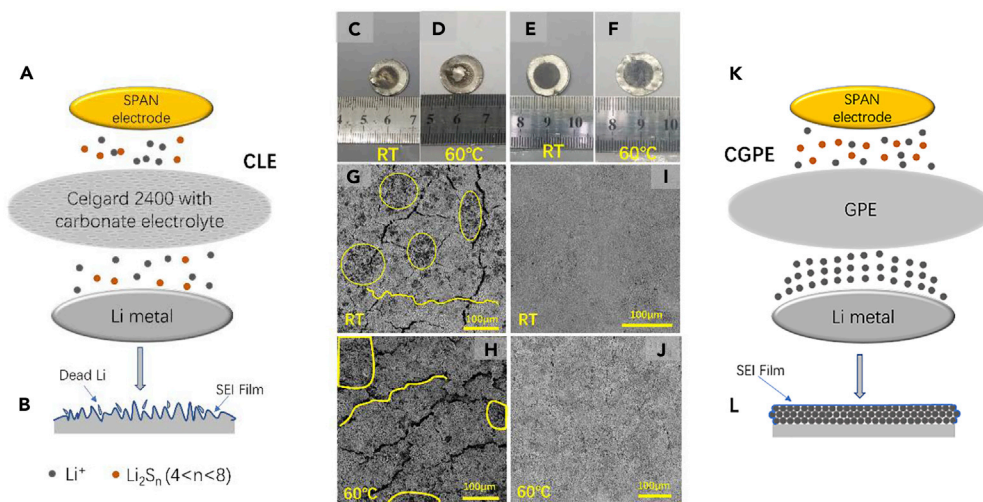
Figure 5. Illustration of the Synergistic Effects of the SPAN Cathode Material and Gel Polymer Electrolyte

(A and B) Scheme of the working principle of CLE.

(C–F) Optical photographs of Li metal in CLE (C and D) and CGPE (E and F) after 100 cycles at room temperature and 60°C.

(G and H) SEM images of Li metal in CLE after 100 cycles at (G) room temperature and (H) 60°C.

(I and J) SEM images of Li metal in CGPE after 100 cycles at (I) room temperature and (J) 60°C.

(K and L) Scheme of the working principle of CGPE. For Figures 5G, 5H, 5I, and 5J, the scale bar is 100 μm.

that the onset voltage of CGPE is higher than that of CLE at each temperature (Figure S10), illustrating the better charge transfer of CGPE than CLE. Analysis of electrochemical impedance spectroscopy leads to consistent results. The impedances of both cells before cycling decrease with the temperature, whereas the impedance of CGPE is much less than that of CLE (Figure S4), suggesting that the GPE would lead to better contact with both electrodes, compared with the commercial separator. Furthermore, as shown in Figure 3E, the impedances of CLE after 100 cycles at 60°C increase significantly compared with that of CGPE; it may be attributed to the dissolution of the polysulfides, and the side reactions of the sulfur in CLE, which formed passivation layer on the electrodes (Gao et al., 2011). This could also lead to degraded performance of CLE. In addition, the employment of the GPE results in a flat Li metal after cycling, even at high temperature (Figures 5E, 5F, 5J, and 5K). The Li metal of CLE becomes rough after 100 cycles at RT, and the roughness becomes more serious when cycling at 60°C (Figures 5G and 5I). In contrast, the surface of Li metal in CGPE is flat and crackless, at both RT and 60°C (Figures 5J and 5K), illustrating that the GPE plays an important role in protecting the Li metal in Li-S batteries, particularly at high temperatures.

DISCUSSION

We have demonstrated a Li-S battery operated in carbonate electrolyte at elevated temperatures, using GPE and SPAN positive electrode materials. The as assembled Li-S battery exhibits high reversible capacity of 520 and 547.8 mAh g^{-1} at 250 mA g^{-1} at 50°C and 60°C, corresponding to 1,368 and 1,441 mAh g_{sulfur}^{-1} based on the sulfur content of the composites, respectively. It exhibits remarkable rate performance with good cycling stability. Combined electrochemical studies with XPS, Raman, SEM, and EDS investigations reveal that the sulfur can be detected on the surface of both lithium metal and positive electrode after cycling, suggesting that the C-S bonds in SPAN are cleaved, and sulfur molecules may be formed with cycling, which results in the dissolution of polysulfides. The synergistic effects of SPAN and the GPE contribute to enhancing the high-temperature performance. The unique structure of SPAN allows the Li-S battery cycled in relatively safe carbonate electrolyte at a relatively high temperature, and the GPE suppresses the polysulfide migration, forms tight contact with both electrodes for good charge transfer, and promises a flat lithium metal after cycling. We hope this study would shed light on the material and system design of high-performance lithium batteries operated at elevated temperatures, including Li-S batteries and beyond.

Limitations of the Study

For the current study, the PAN for the synthesis is commercial and used as received; the content of sulfur, which reacts with PAN to form SPAN, is limited by the particle size and morphology of PAN. Thus it is not

easy to further increase the capacity of the SPAN composite at room temperature in this study. In addition, the areal mass loading of the electrode in this article is low due to the limited electrode preparation technique. It is expected that by optimizing the morphology and properties of the PAN, the amount of the sulfur reacted with PAN can be increased, and the sulfur content in SPAN would increase as well. Thus the capacity of the composites can be further increased. With a modified binder and pressing process, the areal mass loading of the electrode is expected to be improved as well.

SUPPLEMENTAL INFORMATION

Supplemental Information can be found online at https://doi.org/10.1016/j.isci.2019.07.027.

METHODS

All methods can be found in the accompanying Transparent Methods supplemental file.

AUTHOR CONTRIBUTIONS

L.F contributed to the scientific conception. L.F and Y.W designed the experiments. Y.L. and D.Y. executed the experiments. W.Y., Q.H., and Y.Z. assisted the characterizations. L.F, Y.L., and D.Y. analyzed the data, L.F, Y.L, D.Y., and Y.W. wrote the manuscript. All authors discussed the results and commented on the manuscript.

DECLARATION OF INTERESTS

The authors declare no competing interests.

REFERENCES

Agnihotry, S.A., Nidhi, P., and Sekhon, S.S. (2000). Li+ conducting gel electrolyte for electrochromic windows. Solid State Ion. 136, 573–576.

Bruce, P.G., Freunberger, S.A., Hardwick, L.J., and Tarascon, J.-M. (2012). Li–O_2 and Li–S batteries with high energy storage. Nat. Mater. 11, 19.

Burkhardt, S.E., Conte, S., Rodriguez-Calero, G.G., Lowe, M.A., Qian, H., Zhou, W., Gao, J., Hennig, R.G., and Abruña, H.D. (2011). Towards organic energy storage: characterization of 2,5-bis(methylthio)thieno[3,2-b]thiophene. J. Mater. Chem. 21, 9553.

Busche, M.R., Adelhelm, P., Sommer, H., Schneider, H., Leitner, K., and Janek, J. (2014). Systematical electrochemical study on the parasitic shuttle-effect in lithium-sulfur-cells at different temperatures and different rates. J. Power Sources 259, 289–299.

Cha, E., Patel, M.D., Park, J., Hwang, J., Prasad, V., Cho, K., and Choi, W. (2018). 2D MoS_2 as an

efficient protective layer for lithium metal anodes in high-performance Li-S batteries. Nat. Nanotechnol. 13, 337–344.

Chen, T., Zhang, Z., Cheng, B., Chen, R., Hu, Y., Ma, L., Zhu, G., Liu, J., and Jin, Z. (2017). Self-templated formation of interlaced carbon nanotubes threaded hollow Co3S4 nanoboxes for high-rate and heat-resistant lithium-sulfur batteries. J. Am. Chem. Soc. 139, 12710–12715.

Cheng, Z., Xiao, Z., Pan, H., Wang, S., and Wang, R. (2018). Elastic sandwich-type rGO-VS_2/S composites with high tap density: structural and chemical cooperativity enabling lithium-sulfur batteries with high energy density. Adv. Energy Mater. 8, 1702337.

Doan, T.N.L., Ghaznavi, M., Zhao, Y., Zhang, Y.G., Konarov, A., Sadhu, M., Tangirala, R., and Chen, P. (2013). Binding mechanism of sulfur and dehydrogenated polyacrylonitrile in sulfur/polymer composite cathode. J. Power Sources 241, 61–69.

Dong, C., Gao, W., Jin, B., and Jiang, Q. (2018). Advances in cathode materials for high-performance lithium-sulfur batteries. iScience 6, 151–198.

Elazari, R., Salitra, G., Garsuch, A., Panchenko, A., and Aurbach, D. (2011). Sulfur-impregnated activated carbon fiber cloth as a binder-free cathode for rechargeable Li-S batteries. Adv. Mater. 23, 5641–5644.

Fanous, J., Wegner, M., Grimminger, J., Andresen, Ä., and Buchmeiser, M.R. (2011). Structure-related electrochemistry of sulfur-poly(acrylonitrile) composite cathode materials for rechargeable lithium batteries. Chem. Mater. 23, 5024–5028.

Frey, M., Zenn, R.K., Warneke, S., Müller, K., Hintennach, A., Dinnebier, R.E., and Buchmeiser, M.R. (2017). Easily accessible, textile fiber-based sulfurized poly(acrylonitrile) as Li/S cathode material: correlating electrochemical performance with morphology and structure. ACS Energy Lett. 2, 595–604.

Gao, J., Lowe, M.A., Kiya, Y., and Abruna, H.D. (2011). Effects of liquid electrolytes on the charge-discharge performance of rechargeable lithium/sulfur batteries: electrochemical and in-situ X-ray absorption spectroscopic studies. J. Phys. Chem. C *115*, 25132–25137.

Gao, X., Sun, Q., Yang, X., Liang, J., Koo, A., Li, W., Liang, J., Wang, J., Li, R., Holness, F.B., et al. (2019). Toward a remarkable Li-S battery via 3D printing. Nano Energy *56*, 595–603.

Ghazi, Z.A., He, X., Khattak, A.M., Khan, N.A., Liang, B., Iqbal, A., Wang, J., Sin, H., Li, L., and Tang, L. (2017). MoS2/celgard separator as efficient polysulfide barrier for long-life lithium-sulfur batteries. Adv. Mater. *29*, 1606817.

Han, X., Xu, Y., Chen, X., Chen, Y.-C., Weadock, N., Wan, J., Zhu, H., Liu, Y., Li, H., Rubloff, G., et al. (2013). Reactivation of dissolved polysulfides in Li–S batteries based on atomic layer deposition of Al$_2$O$_3$ in nanoporous carbon cloth. Nano Energy *2*, 1197–1206.

Huang, J.-Q., Liu, X.-F., Zhang, Q., Chen, C.-M., Zhao, M.-Q., Zhang, S.-M., Zhu, W., Qian, W.-Z., and Wei, F. (2013). Entrapment of sulfur in hierarchical porous graphene for lithium–sulfur batteries with high rate performance from −40 to 60°C. Nano Energy *2*, 314–321.

Hwa, Y., Seo, H.K., Yuk, J.M., and Cairns, E.J. (2017). Freeze-dried sulfur-graphene oxide-carbon nanotube nanocomposite for high sulfur-loading lithium/sulfur cells. Nano Lett. *17*, 7086–7094.

Hwang, T.H., Jung, D.S., Kim, J.S., Kim, B.G., and Choi, J.W. (2013). One-dimensional carbon-sulfur composite fibers for Na-S rechargeable batteries operating at room temperature. Nano Lett. *13*, 4532–4538.

Jayaprakash, N., Shen, J., Moganty, S.S., Corona, A., and Archer, L.A. (2011). Porous hollow carbon@sulfur composites for high-power lithium-sulfur batteries. Angew. Chem. Int. Ed. *50*, 5904–5908.

Kong, L., Chen, X., Li, B.Q., Peng, H.J., Huang, J.Q., Xie, J., and Zhang, Q. (2018). A bifunctional perovskite promoter for polysulfide regulation toward stable lithium-sulfur batteries. Adv. Mater. *30*, 1705219.

Li, G.R., Ling, M., Ye, Y.F., Li, Z.P., Guo, J.H., Yao, Y.F., Zhu, J.F., Lin, Z., and Zhang, S.Q. (2015). Acacia Senegal-inspired bifunctional binder for longevity of lithium-sulfur batteries. Adv. Energy Mater. *5*, 1500878.

Li, X., Lushington, A., Sun, Q., Xiao, W., Liu, J., Wang, B., Ye, Y., Nie, K., Hu, Y., Xiao, Q., et al. (2016). Safe and durable high-temperature lithium-sulfur batteries via molecular layer deposited coating. Nano Lett. *16*, 3545–3549.

Li, Z., Guan, B.Y., Zhang, J., and Lou, X.W. (2017a). A compact nanoconfined sulfur cathode for high-performance lithium-sulfur batteries. Joule *1*, 576–587.

Li, Y., Fan, J., Zhang, J., Yang, J., Yuan, R., Chang, J., Zheng, M., and Dong, Q. (2017b). A honeycomb-like Co@N-C composite for ultrahigh sulfur loading Li-S batteries. ACS Nano *11*, 11417–11424.

Li, G., Wang, S., Zhang, Y., Li, M., Chen, Z., and Lu, J. (2018a). Revisiting the role of polysulfides in lithium-sulfur batteries. Adv. Mater. *30*, e1705590.

Li, G., Lei, W., Luo, D., Deng, Y.-P., Wang, D., and Chen, Z. (2018b). 3D porous carbon sheets with multidirectional ion pathways for fast and durable lithium-sulfur batteries. Adv. Energy Mater. *8*, 1702381.

Li, X., Banis, M., Lushington, A., Yang, X., Sun, Q., Zhao, Y., Liu, C., Li, Q., Wang, B., Xiao, W., et al. (2018c). A high-energy sulfur cathode in carbonate electrolyte by eliminating polysulfides via solid-phase lithium-sulfur transformation. Nat. Commun. *9*, 4509.

Li, Z., Zhang, J., Lu, Y., and Lou, X.W.D. (2018d). A pyrolyzed polyacrylonitrile/selenium disulfide composite cathode with remarkable lithium and sodium storage performances. Sci. Adv. *4*, eaat1687.

Liu, Y., Wang, W., Wang, J., Zhang, Y., Zhu, Y., Chen, Y., Fu, L., and Wu, Y. (2018). Sulfur nanocomposite as a positive electrode material for rechargeable potassium-sulfur batteries. Chem. Commun.(Camb.) *54*, 2288–2291.

MacDiarmid, A.G. (2001). Synthetische Metalle: eine neue Rolle für organische polymere. Angew. Chem. Int. Ed. *113*, 2649–2659.

Otero, T.F., and Cantero, I. (1999). Conducting polymers as positive electrodes in rechargeable lithium-ion batteries. J. Power Sources *81*, 838–841.

Seh, Z.W., Sun, Y., Zhang, Q., and Cui, Y. (2016). Designing high-energy lithium-sulfur batteries. Chem. Soc. Rev. *45*, 5605–5634.

Service, R.F. (2018). Lithium-sulfur batteries poised for leap. Science *359*, 1080–1081.

Song, J., Gordin, M.L., Xu, T., Chen, S., Yu, Z., Sohn, H., Lu, J., Ren, Y., Duan, Y., and Wang, D. (2015). Strong lithium polysulfide chemisorption on electroactive sites of nitrogen-doped carbon composites for high-performance lithium-sulfur battery cathodes. Angew. Chem. Int. Ed. *54*, 4399–4403.

Sun, J., Sun, Y., Pasta, M., Zhou, G., Li, Y., Liu, W., Xiong, F., and Cui, Y. (2016). Entrapment of polysulfides by a black-phosphorus-modified separator for lithium-sulfur batteries. Adv. Mater. *28*, 9797–9803.

Umeshbabu, E., Zheng, B., and Yang, Y. (2019). Recent progress in all-solid-state Lithium−Sulfur batteries using high Li-ion conductive solid electrolytes. Electrochem. Energy Rev. *2*, 199–230.

Vondrák, J., Sedlaříková, M., Velická, J., Klápště, B., Novák, V., and Reiter, J. (2001). Gel polymer electrolytes based on PMMA. Electrochim. Acta *46*, 2047–2048.

Wang, J.L., Yang, J., Xie, J.Y., and Xu, N.X. (2002). A novel conductive polymer-sulfur composite cathode material for rechargeable lithium batteries. Adv. Mater. *14*, 963–965.

Wang, J., Yang, J., Wan, C., Du, K., Xie, J., and Xu, N. (2003). Sulfur composite cathode materials for rechargeable lithium batteries. Adv. Funct. Mater. *13*, 487–492.

Wang, H., Wang, C., Matios, E., and Li, W. (2018a). Facile stabilization of sodium metal anode with additives: unexpected key role of sodium polysulfide and adverse effect of sodium nitrate. Angew. Chem. Int. Ed. *57*, 7734–7737.

Wang, W., Cao, Z., Elia, G.A., Wu, Y., Wahyudi, W., Abou-Hamad, E., Emwas, A.-H., Cavallo, L., Li, L.J., and Ming, J. (2018b). Recognizing the mechanism of sulfurized polyacrylonitrile cathode materials for Li−S batteries and beyond in Al−S batteries. ACS Energy Lett. *3*, 2899–2907.

Wei, S., Ma, L., Hendrickson, K.E., Tu, Z., and Archer, L.A. (2015). Metal-sulfur battery cathodes based on PAN-sulfur composites. J. Am. Chem. Soc. *137*, 12143–12152.

Xin, S., Gu, L., Zhao, N.H., Yin, Y.X., Zhou, L.J., Guo, Y.G., and Wan, L.J. (2012). Smaller sulfur molecules promise better lithium-sulfur batteries. J. Am. Chem. Soc. *134*, 18510–18513.

Yang, X., Chen, Y., Wang, M., Zhang, H., Li, X., and Zhang, H. (2016). Phase inversion: a universal method to create high-performance porous electrodes for nanoparticle-based energy storage devices. Adv. Funct. Mater. *26*, 8427–8434.

Yang, X., Zhang, H., Chen, Y., Yu, Y., Li, X., and Zhang, H. (2017). Shapeable electrodes with extensive materials options and ultra-high loadings for energy storage devices. Nano Energy *39*, 418–428.

Yang, X., Li, X., Adair, K., Zhang, H., and Sun, X. (2018a). Structural design of lithium–sulfur batteries: from fundamental research to practical application. Electrochem. Energy Rev. *1*, 239–293.

Yang, X., Yu, Y., Lin, X., Liang, J., Adair, K., Zhao, Y., Wang, C., Li, X., Sun, Q., Zhang, H., et al. (2018b). Multi-functional nanowall arrays with unrestricted Li$^+$ transport channels and an integrated conductive network for high-areal-capacity Li–S batteries. J. Mater. Chem. A *6*, 22958–22965.

Yu, X.G., Xie, J.Y., Yang, J., Huang, H.J., Wang, K., and Wen, Z.S. (2004). Lithium storage in conductive sulfur-containing polymers. J. Electroanal. Chem. (Lausanne) *573*, 121–128.

Zhong, Y., Yin, L., He, P., Liu, W., Wu, Z., and Wang, H. (2018). Surface chemistry in cobalt phosphide-stabilized lithium-sulfur batteries. J. Am. Chem. Soc. *140*, 1455–1459.

Zhou, W., Yu, Y., Chen, H., DiSalvo, F.J., and Abruna, H.D. (2013). Yolk-shell structure of polyaniline-coated sulfur for lithium-sulfur batteries. J. Am. Chem. Soc. *135*, 16736–16743.

Zhou, G., Paek, E., Hwang, G.S., and Manthiram, A. (2015). Long-life Li/polysulphide batteries with high sulphur loading enabled by lightweight three-dimensional nitrogen/sulphur-codoped graphene sponge. Nat. Commun. *6*, 7760.

Zhou, J., Qian, T., Xu, N., Wang, M., Ni, X., Liu, X., Shen, X., and Yan, C. (2017). Selenium-DOPED cathodes for lithium-organosulfur batteries with greatly improved volumetric capacity and coulombic efficiency. Adv. Mater. *29*, 1701294.

Supplemental Information

Synergy of Sulfur/Polyacrylonitrile

Composite and Gel Polymer Electrolyte

Promises Heat-Resistant Lithium-Sulfur Batteries

Yu Liu, Dezhi Yang, Wenqi Yan, Qinghong Huang, Yusong Zhu, Lijun Fu, and Yuping Wu

METHODS

Synthesis

The SPANs were prepared via facile one-pot solid-state reaction During the reaction, the mixture of PAN (Sigma, M_w=150000) and sulfur (Aladdin, ⩾99.5%) with a weight ratio of 1:4 were heated at 450 ℃ for 5 h under continuous argon gas flow. The PAN was obtained after a cyclization process during the heat treatment. Polyvinylidene fluoride (PVDF, 1.5g, M_w=370000, AR, Arkema) and polymethyl methacrylate (PMMA, 1.5g, M_w=800000, AR, Aladdin) was dissolved into N-methyl-2-pyrrolidinone (NMP, 8.5g, AR, Aladdin) to form homogeneous solution, respectively. Firstly, PVDF solution was cast onto a pre-heated glass plate and kept at 80 ℃ for 6h to evaporate the solvent. Then, PMMA solution was cast onto the thin PVDF layer and dried at 80 ℃ in air for 6h. Again, the PVDF solution was cast onto the PMMA layer. After the evaporation of solvent, a dense gel polymer membrane with thickness of 20-21 μm was successfully achieved.

Material Characterizations

Field emission scanning electron microscopy images and element mapping images were obtained with a JSM-7800 field emission scanning electron microscope (FESEM). Transmission electron microscopy (TEM) analysis was performed on a JEM-2100 transmission electron microscope operating at 200 kV. XPS (Kratos AXIS Ultra DLD) was applied to study the change of valence state of elements in SPAN. The Raman spectra were collected using an alpha 300 M+ Raman Microscope. For characterization of the samples after cycling, they were protected in Argon atmosphere for Raman and XPS measurements. There is a short air exposure during the transfer process for the FESEM and EDS measurements. The content of S was determined via organic element analyzer (Elementar vario EL cube) and EDS mapping.

Electrochemical Characterization

The cathode was prepared by mixing SPAN powder, carbon black and PVDF (polyvinylidene fluoride) binder in NMP (N-methyl pyrrolidinone) solvent at a weight

ratio of 80:10:10 and uniformly spread on pure aluminum foil and then dried at 60 °C for 24 h. The cathode electrode was punched into coins with a diameter of 10 mm and commercial lithium foil with a diameter of 15.6 mm was used as the counter electrode. For CLE, a Celgard2400 membrane was used as separator and freshly 1 M $LiPF_6$ in a mixture of ethylene carbonate and dimethyl carbonate (EC/DMC=1/1, v/v) as electrolyte. For CGPE, the polymer membrane with 1 M $LiPF_6$ in a mixture of ethylene carbonate and dimethyl carbonate (EC/DMC=1/1, v/v) was used as electrolyte. The dosage of carbonate electrolyte is 30 and 25 μL for CGPE and CLE, respectively. The loading of the nanocomposites in the cathode was 1 mg cm^{-2}. The cells were galvanostatically cycled between 1.0-3.0 V (vs Li/Li^+) on a multi-channel battery tester (Land CT2001A) under different current densities. The electrochemical impedance spectra (EIS) were measured by a CHI 760 (Shanghai, China) electrochemical workstation in the frequency range of 100 kHz to 0.1 Hz.

The SPAN/GPM/Li, SPAN/Celgard 2400/Li, coin cells after designated cyclic tests were transferred into the glovebox and dissembled for further examination. The Li metal and the positive electrode were repeatedly rinsed with DMC and vacuum dried at 60 ℃ for 2 h to remove the residual solvent. The morphology of Li anodes and membranes were characterized by SEM at 10 kV and 5 kV, respectively. The capacities of the coin cells were calculated according to the mass of the composite.
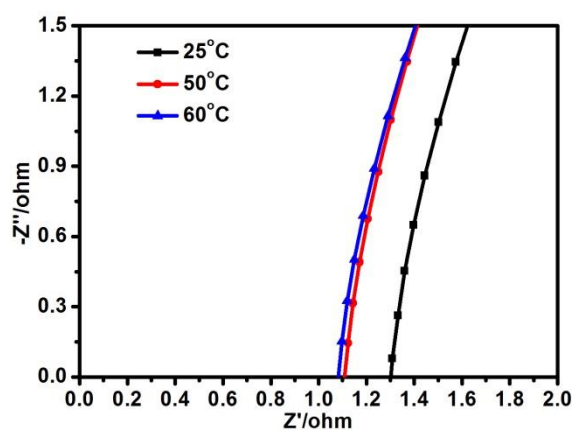
Figure S1. Electrochemical impedance spectroscopy of the symmetrical SS/GPE/SS cell at different temperatures, Related to Figure 1.

The ionic conductivity of the GPE at different temperature was evaluated by the electrochemical impedance spectroscopy (EIS). Typically, a stainless steel (SS)/CGPE/stainless steel (SS) symmetrical cell was assembled and then tested in a CHI 604e electrochemical workstation. The EIS measurement was conducted at the frequency between 1 Hz-100 kHz with the applied voltage amplitude of 5 mV. The ionic conductivity was calculated from the equation(Zhu et al., 2014):

$$\sigma = L / (R_b \times A)$$

where σ is the ionic conductivity, L represents the thickness of the CGPE membrane, R_b is the bulk resistance obtained from the EIS measurement and A stands for the contact area between the stainless steel and the CGPE.
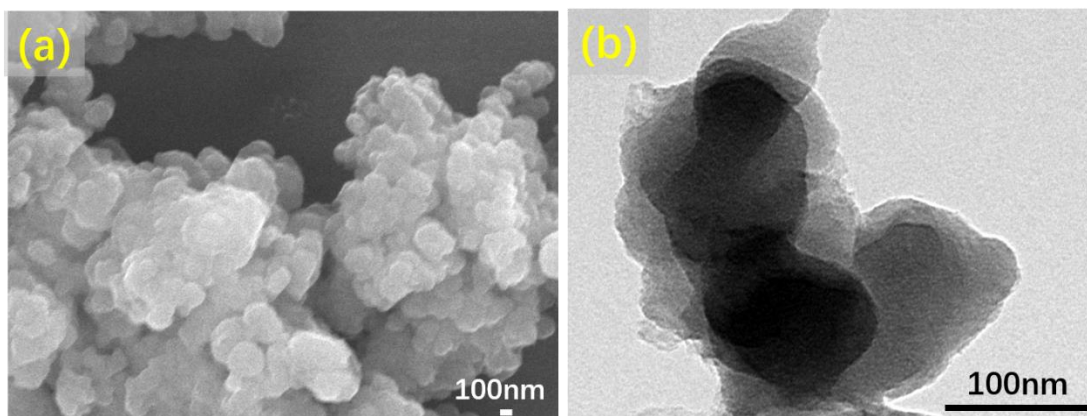
Figure S2. Morphology characterization of SPAN. (a) FESEM image and (b) TEM image, Related to Figure 2 and Figure 3.
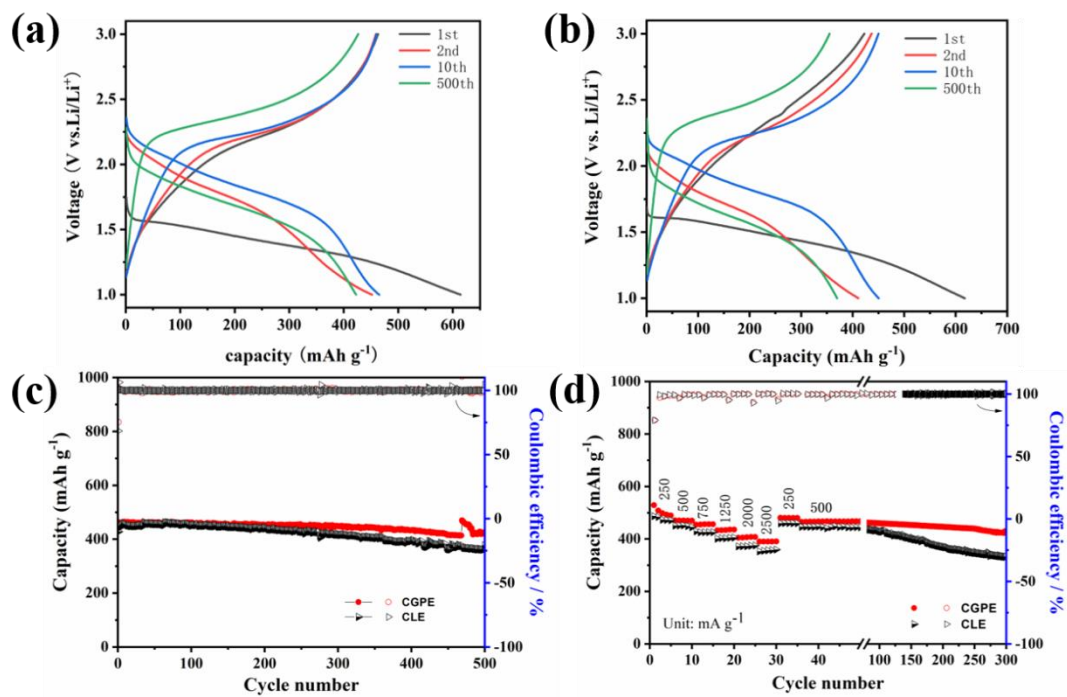
Figure S3. Electrochemical characterization and performance of the SPAN electrodes in CLE and CGPE. (a) Galvanostatic charge/discharge voltage profile of CGPE at room temperature. (b) Galvanostatic charge/discharge voltage profile of CLE at room temperature. (c) Cycling performance of CGPE and CLE at 500 mA g^{-1}. (d) Rate performance of CGPE and CLE for Li-S batteries, Related to Figure 2 and Figure 3.
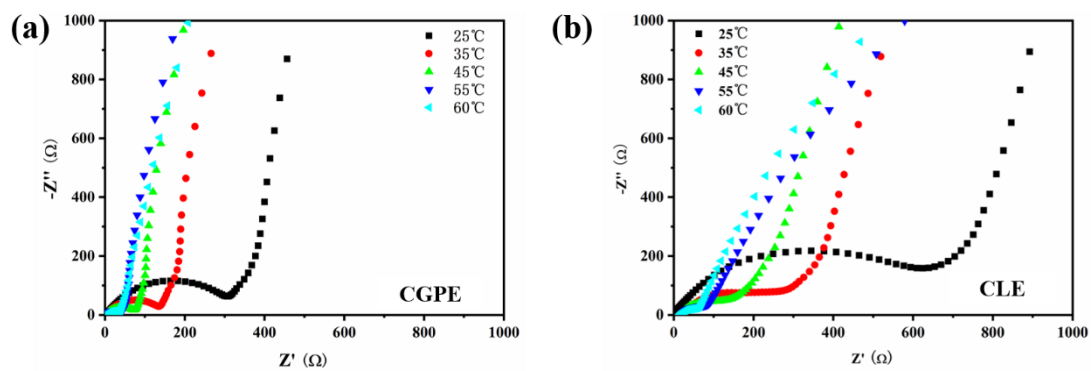
Figure S4. Nyquist plots of (a) CGPE and (b) CLE before cycling at different temperatures from 25 to 60°C, Related to Figure 2 and Figure 3.
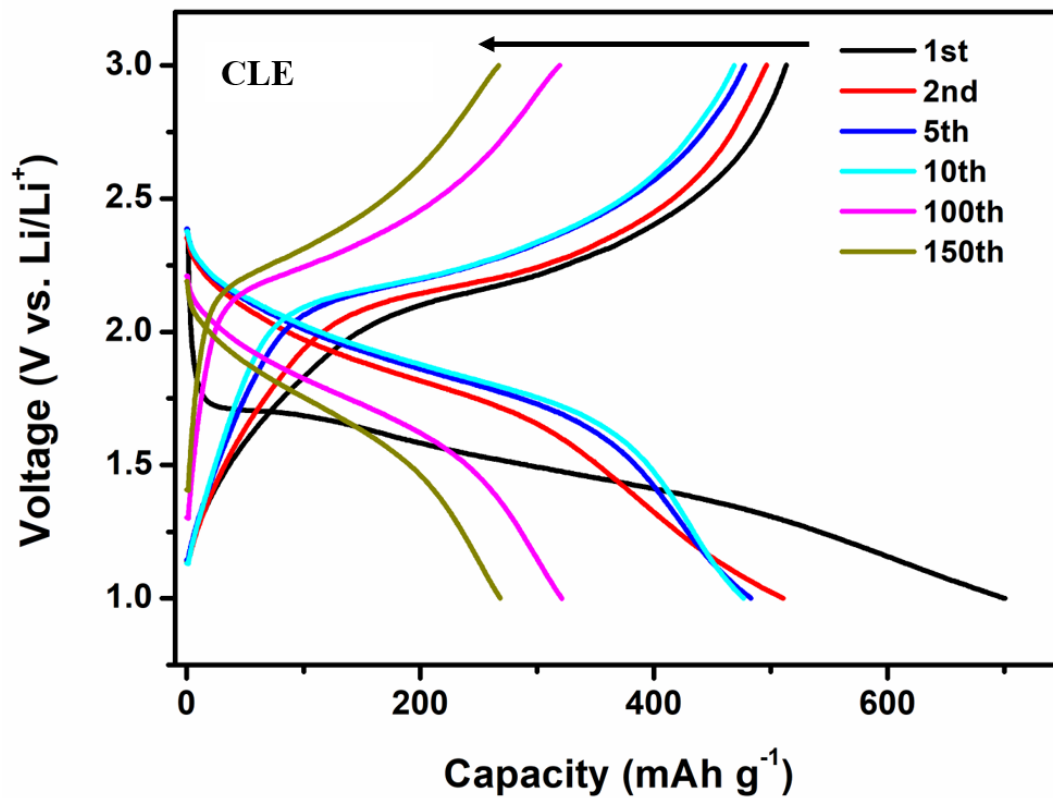
Figure S5. Galvanostatic charge/discharge voltage profiles of CLE at 50 °C at 250 mA g^{-1}, Related to Figure 2.
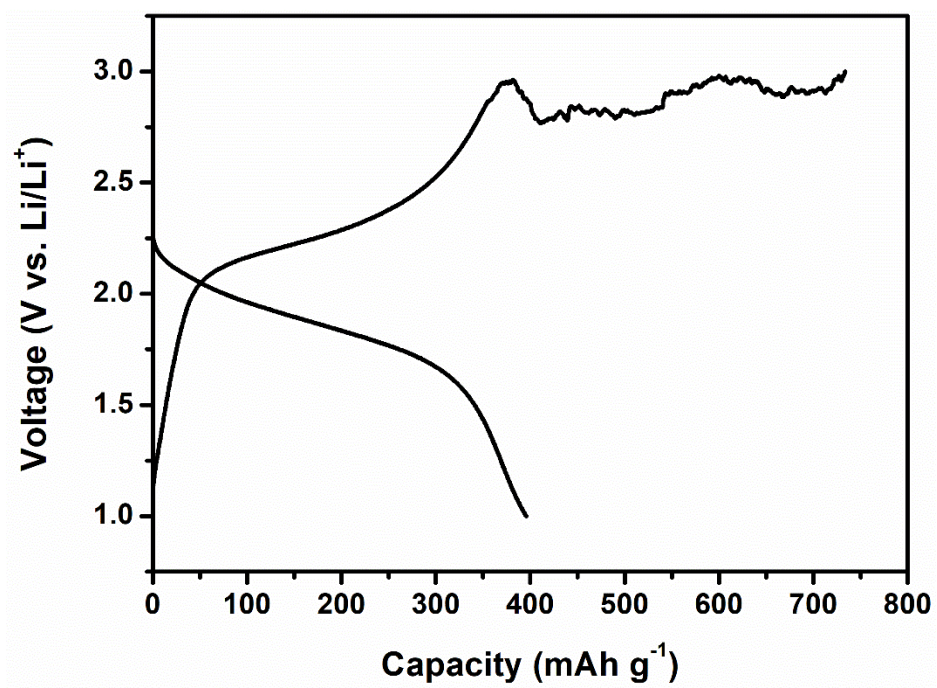
Figure S6. Charge/discharge galvanostatic profile of CLE at 60 ℃, Related to Figure 3.
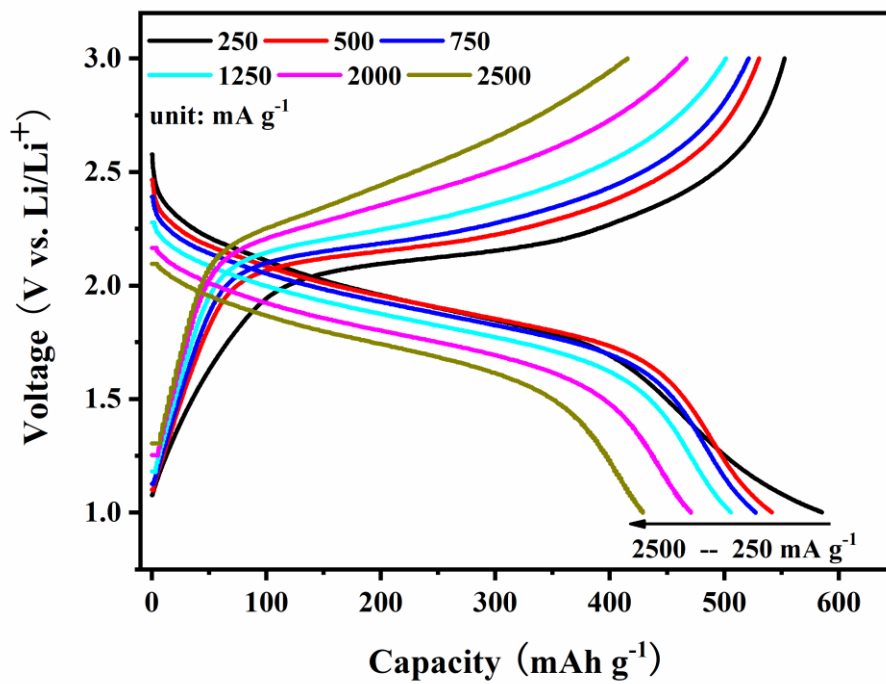
Figure S7. Galvanostatic charge/discharge voltage profiles of CGPE at various current densities from 250 to 2500 mA g^{-1} at 60 ^{o}C, Related to Figure 3.
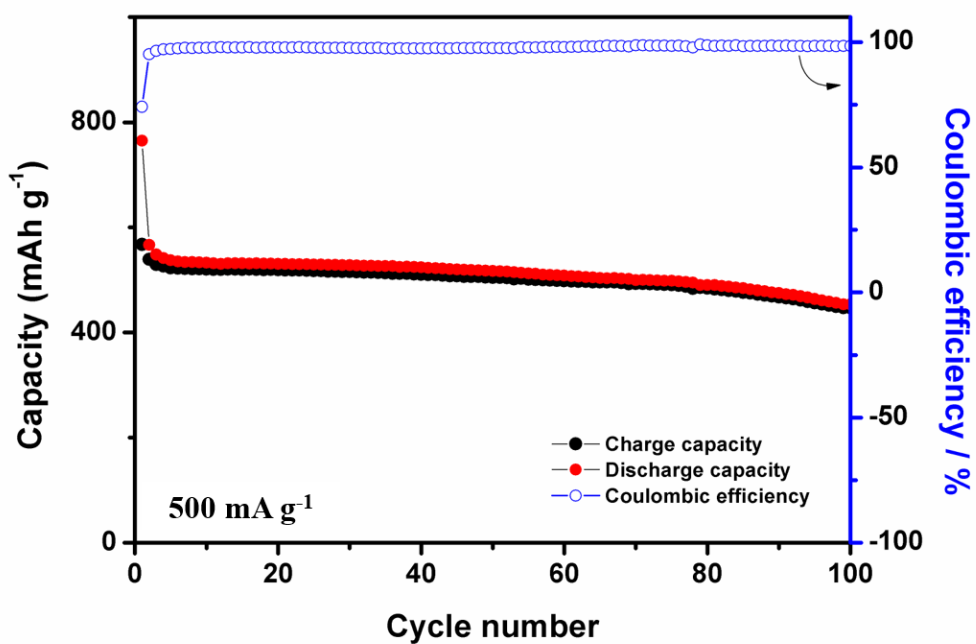
Figure S8. Cycling performance of CGPE under 60°C at 500 mA g^{-1}, Related to Figure 3.
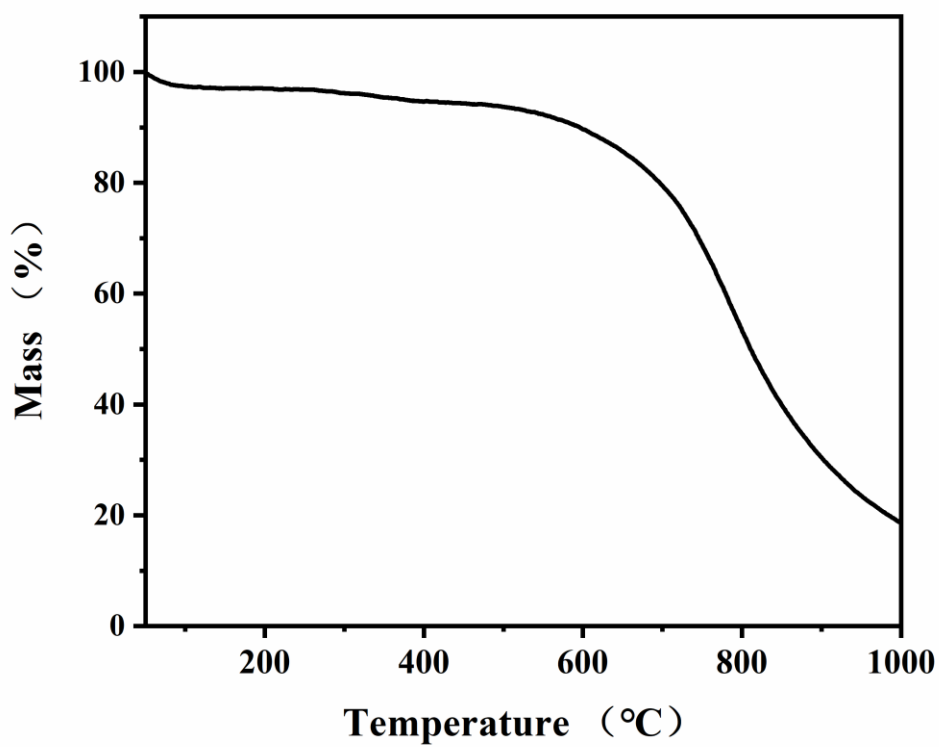
Figure S9. TG analysis of SPAN under argon atmosphere with a temperature increase rate of 10 K min^{-1}, Related to Table 1 and Table 2.
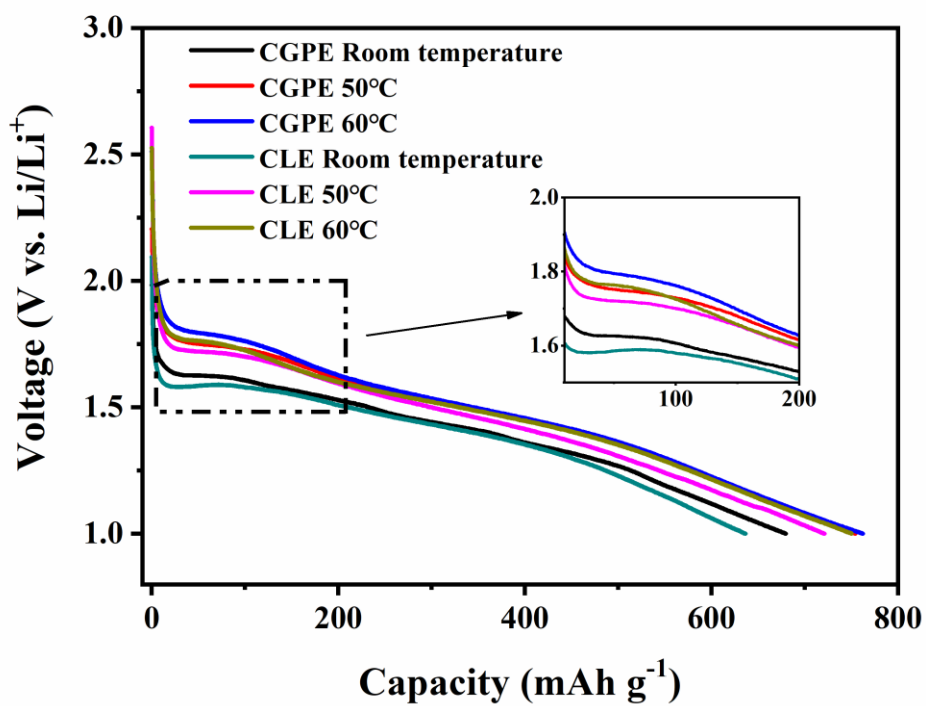
Figure S10. The first discharge profile of CGPE and CLE at different temperatures at 250mA g^{-1}, Related to Figure 2 and Figure 3.

Table S1. Cycling performance of SPAN cathode with different gel electrolyte at room temperatures, Related to Figure 2 and Figure 3.

	Cycle performance Capacity normalized by the content of sulfur	Gel polymer	Ref
1	1122.7 mAh/g after 500 cycles at 500 mA/g (retention: 92.2%)	CGPE (PVDF PMMA)	This Work
2	1123.4 mAh/g after 50 cycles at 0.2 mA/cm^2(retention: 70.6%)	PVDF-HFP	(Wang et al., 2002)
3	1123.4 mAh/g after 50 cycles at 0.3 mA/cm^2(retention: 70.6%)	PVDF-HFP Nano SiO$_2$	(Wang et al., 2003)
4	1050 mAh/g after 100 cycles at 335 mA/g (retention: 88%)	GPE (PVDF-HFP functionalized PMMA)	(Jeddi et al., 2013)
5	1143 mAh/g after 100 cycles at 335 mA/g (retention: 69.4%)	CPE (PVDF-HFP f-PMMA MPS)	(Jeddi et al., 2014)
6	1071 mAh/g after 100 cycles at 167 mA/g (retention: 75.5%)	GPE (PVDF-HFP PMMA MMT)	(Zhang et al., 2014)
7	1276 mAh/g after 50 cycles at 60 mA/g (retention: ～63.8%)	DGE (EC DMC)	(Wu et al., 2014)

Table S2. Cycling performance of different Li-S batteries at high temperatures, Related to Figure 2 and Figure 3.

	Cycle performance Capacity normalized by the content of sulfur	Temperature	Electrolyte	Ref
1	1176 mAh/g after 100 cycles at 500 mA/g (retention: 78.8%)	60℃	Gel polymer electrolyte (with LiPF$_6$ in carbonate solvent)	This work
	1236 mAh/g after 200 cycles at 500 mA/g (retention: 85%)	50℃		
2	661mAh/g after 50 cycles at 167.5 mA/g (retention: 62.7%)	55℃	LiPF$_6$ in carbonate solvent	(Li et al., 2016)
3	650 mAh/g after 10 cycles at 167.5 mA/g (only test 10 cycles)	45℃	LiTFSI in ether solvent	(Gordin et al., 2014)
4	250 mAh/g after 50 cycles at 167.5 mA/g	45℃	LiTFSI in ether solvent	(Busche et al., 2014)
5	350 mAh/g after 150 cycles at 3350 mA/g	70℃	LiTFSI in ether solvent	(Kim et al., 2013)
6	450 mAh g^{-1} after 80 cycles at 1675 mA/g	60℃	LiTFSI in ether solvent	(Huang et al., 2013)

Table S3. The element contents on surface of the positive electrode in Li-S batteries at different temperatures and cycle states via XPS test, Related to Table 1 and Table 2.

Electrode			Content (*ac*%)		
membrane	Test temperature	Electrode state	C	S	N
CLE	Room temperature	1th Discharge 1.0V	99.72	0.28	0
		1th Charge 3.0V	98.47	1.09	0.44
		500th Discharge 1.0V	99.56	0.44	0
		500th Charge 3.0V	99.49	0.51	0
	60°C	100th Charge 3.0V	99.83	0.17	0
CGPE	60°C	100th Charge 3.0V	99.44	0.21	0.35

References

Zhu, Y., Xiao, S., Shi, Y., Yang, Y., Hou, Y., and Wu, Y. (2014). A Composite Gel Polymer Electrolyte with High Performance Based on Poly(Vinylidene Fluoride) and Polyborate for Lithium Ion Batteries. Adv. Energy Mater. 4, 1300647.

Wang, J. L., Yang, J., Xie, J. Y., and Xu, N. X. (2002). A novel conductive polymer-sulfur composite cathode material for rechargeable lithium batteries. Adv. Mater. 14, 963-965.

Wang, J., Yang, J., Wan, C., Du, K., Xie, J., and Xu, N. (2003). Sulfur Composite Cathode Materials for Rechargeable Lithium Batteries. Adv. Funct. Mater. 13, 487-492.

Jeddi, K., Ghaznavi, M., and Chen, P. (2013). A novel polymer electrolyte to improve the cycle life of high performance lithium–sulfur batteries. J. Mater. Chem. A 1, 2769–2772.

Jeddi, K., Sarikhani, K., Qazvini, N. T., and Chen, P. (2014). Stabilizing lithium/sulfur batteries by a composite polymer electrolyte containing mesoporous silica particles. J. Power Sources 245, 656-662.

Zhang, Y., Zhao, Y., Bakenov, Z., Gosselink, D., and Chen, P. (2014). Poly(vinylidene fluoride-co-hexafluoropropylene)/poly(methylmethacrylate)/nanoclay composite gel polymer electrolyte for lithium/sulfur batteries. Journal of Solid State Electrochemistry 18, 1111-1116.

Wu, B., Liu, Q., Mu, D., Ren, Y., Li, Y., Wang, L., Xu, H., and Wu, F. (2014). New Desolvated Gel Electrolyte for Rechargeable Lithium Metal Sulfurized Polyacrylonitrile (S-PAN) Battery. J. Phys. Chem. C 118, 28369-28376.

Li, X., Lushington, A., Sun, Q., Xiao, W., Liu, J., Wang, B., Ye, Y., Nie, K., Hu, Y., Xiao, Q., Li, R., Guo, J., Sham, T. K., and Sun, X. (2016). Safe and Durable High-Temperature Lithium-Sulfur Batteries via Molecular Layer Deposited Coating. Nano Lett. 16, 3545-3549.

Gordin, M. L., Dai, F., Chen, S., Xu, T., Song, J., Tang, D., Azimi, N., Zhang, Z., and Wang, D. (2014). Bis(2,2,2-trifluoroethyl) ether as an electrolyte co-solvent for mitigating self-discharge in lithium-sulfur batteries. ACS Appl. Mater. Interfaces 6, 8006-8010.

Busche, M. R., Adelhelm, P., Sommer, H., Schneider, H., Leitner, K., and Janek, J. (2014). Systematical electrochemical study on the parasitic shuttle-effect in lithium-sulfur-cells at different temperatures and different rates. J. Power Sources 259, 289-299.

Kim, H., Lee, J. T., and Yushin, G. (2013). High temperature stabilization of lithium–sulfur cells with carbon nanotube current collector. J. Power Sources 226, 256-265.

Huang, J.-Q., Liu, X.-F., Zhang, Q., Chen, C.-M., Zhao, M.-Q., Zhang, S.-M., Zhu, W., Qian, W.-Z., and Wei, F. (2013). Entrapment of sulfur in hierarchical porous graphene for lithium–sulfur batteries with high rate performance from −40 to 60°C. Nano Energy 2, 314-321.